Bright contrast imaging of carbon nanofiber-substrate interface

Makoto Suzuki,[a] Yusuke Ominami, Quoc Ngo, and Cary Y. Yang
Center for Nanostructures, Santa Clara University, 500 El Camino Real, Santa Clara, California 95053

Toshishige Yamada, Alan M. Cassell, and Jun Li
Center for Nanotechnology, NASA Ames Research Center, Moffett Field, California 94035

(Received 8 August 2006; accepted 26 September 2006; published online 17 November 2006)

We present the contrast mechanisms of scanning electron microscopy (SEM) for visualizing the interface between carbon nanofibers (CNFs) and the underlying substrate. SEM imaging with electron beam energies higher than a certain threshold provides different image contrasts depending on whether CNFs are in contact with the substrate or suspended above the substrate. CNFs with diameters ranging from 25 to 250 nm are examined with various electron beam energies. It is found that the threshold energy corresponds to the energy required to penetrate the CNF and its dependence on CNF diameter can be understood using the theory of electron range. This knowledge will be quite useful for interface imaging of all nanostructure devices. © *2006 American Institute of Physics*. [DOI: 10.1063/1.2382718]

I. INTRODUCTION

The technology of positioning control for nanoscale materials has been recently improved. Positioning and directional control of horizontally grown carbon nanotubes (CNTs) using chemical vapor deposition[1] (CVD) and vertically aligned carbon nanofibers (CNFs) using plasma-enhanced CVD (PECVD) (Refs. 2 and 3) increases the potential for applications into next-generation interconnect materials for electronic devices.[4–6] Additionally, the mechanical positioning method of CNTs to avoid heating the device during fabrication has been reported recently.[7]

While these techniques hold great promise for applications towards future device technologies, the proper test and inspection techniques should be developed concurrently to enable high production yield. Recent studies reveal that the electrical properties of CNTs and CNFs strongly depend on their configuration, particularly the thermal dissipation via the support material on which they rest. Thermal effects strongly influence both *I-V* characteristics[8,9] and current-carrying capacity.[10] Even though these materials are prepared on substrates for device fabrication, some of them are placed with only a portion of their sidewalls in contact with the substrate. This partial contiguity between nanofiber and substrate can adversely affect the heat dissipation and result in poor device performance and reliability.

Although direct imaging of the interface between the substrate and CNFs resting on it can be carried out with scanning electron microscopy (SEM) by tilting the sample substrate and imaging with a grazing beam, this causes poor image resolution due to the large working distance and results in low inspection efficiency for integrated devices on wafers because of the small in-focus area within the electron beam scanning field. Cross sectional imaging with transmission electron microscopy is another powerful tool for high-resolution imaging of interface, but this is more useful for detailed characterization after defect detection and defect isolation.

Recently, contrast mechanisms for visualizing single-walled carbon nanotubes (SWNTs) on insulating substrate using SEM have been reported.[11,12] In Ref. 11, strong bright contrast was observed around SWNTs in contact with substrate, using current from electron-beam-induced conductivity (EBIC). In this case, the insulating substrate attaching the SWNTs showed bright contrast. In Ref. 12, electron beam irradiation created an electric potential difference between SWNTs and the substrate, resulting in bright voltage contrast.[13] These contrast mechanisms were observed for insulating substrates.

Here, we demonstrate a different contrast mechanism by which SEM image contrast with normal incident beam contains information about the interface between CNFs and a substrate, thereby providing an efficient interface imaging method without beam tilting. We examine the SEM contrast of CNFs with various diameters by changing the electron beam energy. We show that the contrast mechanism is well explained by considering electron penetration into the fibers and edge contrast of SEM image formation.

II. EXPERIMENT

CNFs are grown by PECVD on Ni/Ti/Si wafer with a gas mixture of NH_3:C_2H_2 (4:1) at 4 Torr. The thin Ni film serves as a catalyst for CNF growth. Details of the reaction conditions are described elsewhere.[2] The structure of CNFs grown by PECVD is well studied with transmission electron microscopy (TEM) or scanning transmission electron microscopy (STEM) and characterized as having stacked cup-shaped morphology.[3,14] As-grown CNFs are removed from the wafer with ultrasound agitation and dispersed onto Si substrates. The SEM used for this study is a Hitachi S-4800 field emission SEM with beam deceleration unit, which makes ultralow energy imaging possible down to 100 eV.

[a]Author to whom correspondence should be addressed; electronic mail: m1suzuki@scu.edu

 © 2006 American Institute of Physics

Downloaded 12 Feb 2008 to 129.210.95.1. Redistribution subject to AIP license or copyright; see http://jap.aip.org/jap/copyright.jsp

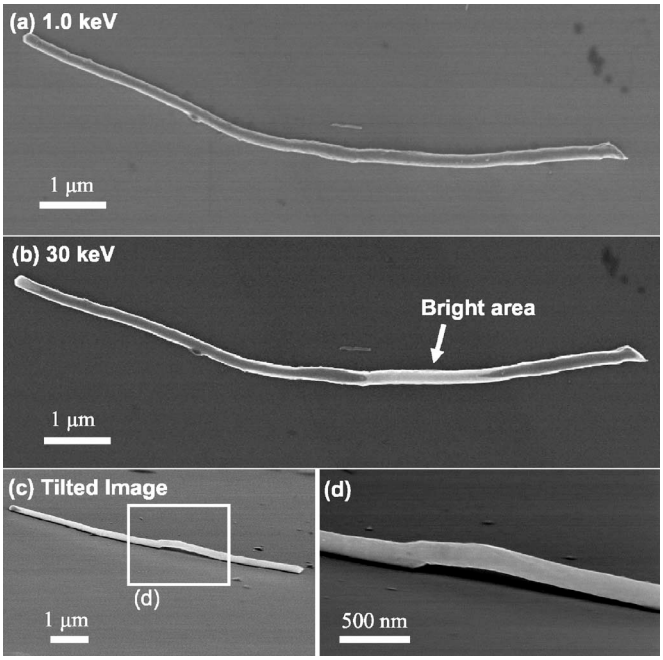

FIG. 1. SEM images of a dispersed CNF on Si substrate with beam energy of (a) 1 keV and (b) 30 keV. Bright contrast observed in (b) on the right portion of the CNF indicates the CNF separation from the substrate (indicated by white arrow). (c) 80° tilted SEM image of same CNF as (a) and (b). (d) Magnified image of the defective portion of (c).

Signal detectors are placed above the objective lens for efficient secondary electron collection [through-the-lens (TTL) detector] and at the side of the specimen chamber [Everhart-Thornley (ET) detector]. Efficient secondary electron collection, irrespective of their emitting direction, by the TTL detector is achieved with electron trapping by the magnetic field of snorkel type objective lens and extraction electric field above the sample.[15] SEM images presented below are mostly captured with the TTL detector, thus the image contrast is formed mainly by secondary electrons (SEs) emitted from the sample with kinetic energies below 50 eV.

III. RESULTS AND DISCUSSION

In Fig. 1(a), the SEM image of a dispersed CNF on Si substrate is shown, using an electron beam energy of 1 keV. The CNF shows uniform contrast along its body, looking as though it is uniformly placed on the substrate. The same CNF exhibits nonuniform SEM contrast when scanned with an electron beam energy of 30 keV, as shown in Fig. 1(b). By imaging with a grazing beam (80° off the substrate normal), it is found that the bright area corresponds to the region where the CNF is not in contact with the underlying Si substrate [shown in Figs. 1(c) and 1(d)], creating a possible failure mechanism due to poor heat dissipation when used for current carrying devices. Indeed, it is seen in Ref. 8 that the current-carrying capacity of a suspended quasi-one-dimensional structure is reduced, likely due to the heat dissipation problem between the nanostructure and the contact substrate. Other dispersed CNF samples are shown in Fig. 2(a). These CNFs are not isolated but overlapping one another. This sort of samples provide the ideal configuration for studying the unique SEM contrast observed above, because

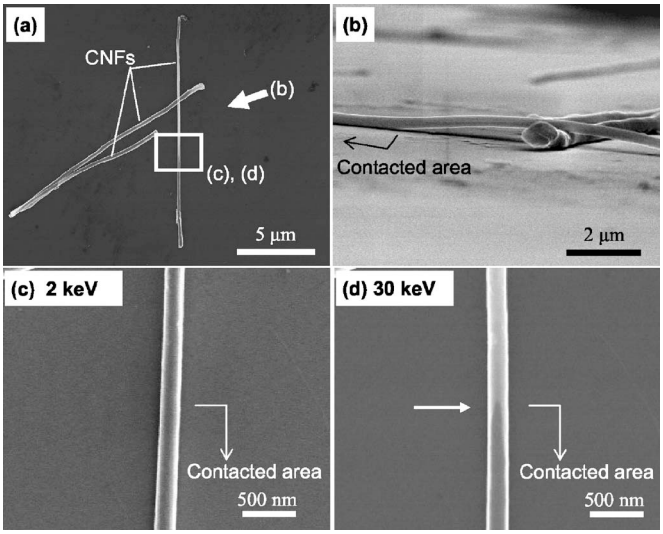

FIG. 2. (a) SEM image of CNFs dispersed on Si substrate. The white arrow indicates the direction of the grazing electron beam in (b). (b) 80° tilted SEM image of (a). (c) Magnified SEM image of a CNF with electron beam energy of 2 keV. (d) Magnified SEM image of a CNF with electron beam energy of 30 keV. The arrow indicates the position of contrast change.

the overlapping CNFs have both the portion in contact with the substrate and that suspended above it, as shown in Fig. 2(b), and this partial contact can be easily deduced without tilting the substrate. Here, the same phenomenon is observed: uniform contrast with low-energy beam [2 keV, Fig. 2(c)] and bright contrast in the noncontacted region with high-energy beam [30 keV, Fig. 2(d)].

In Figs. 3(a) and 3(b), we show the beam energy dependence of SEM contrast of overlapped CNFs with diameters 250 and 74 nm, respectively. At the highest beam energy for each CNF shown in the left column, a clear contrast change is observed depending on whether or not the irradiated part of CNFs is in contact with the substrate. While the contrast for the thicker fiber in Fig. 3(a) is smeared out below 10 keV and becomes uniform at 3 keV, the thinner fiber in Fig. 3(b) exhibits similar phenomenon at 3 and 1 keV. This means that the contrast change observed here has strong correlation with CNF diameter and electron beam energy.

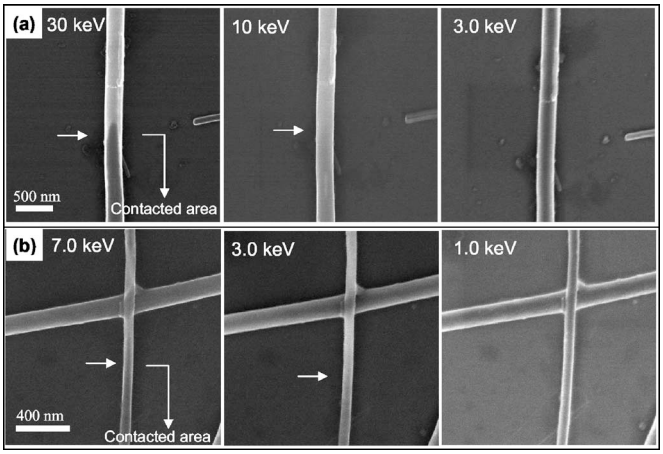

FIG. 3. Beam energy dependence of CNF image contrast for (a) 250 nm and (b) 74 nm diameter CNFs. The arrows indicate the position of contrast change.

Downloaded 12 Feb 2008 to 129.210.95.1. Redistribution subject to AIP license or copyright; see http://jap.aip.org/jap/copyright.jsp

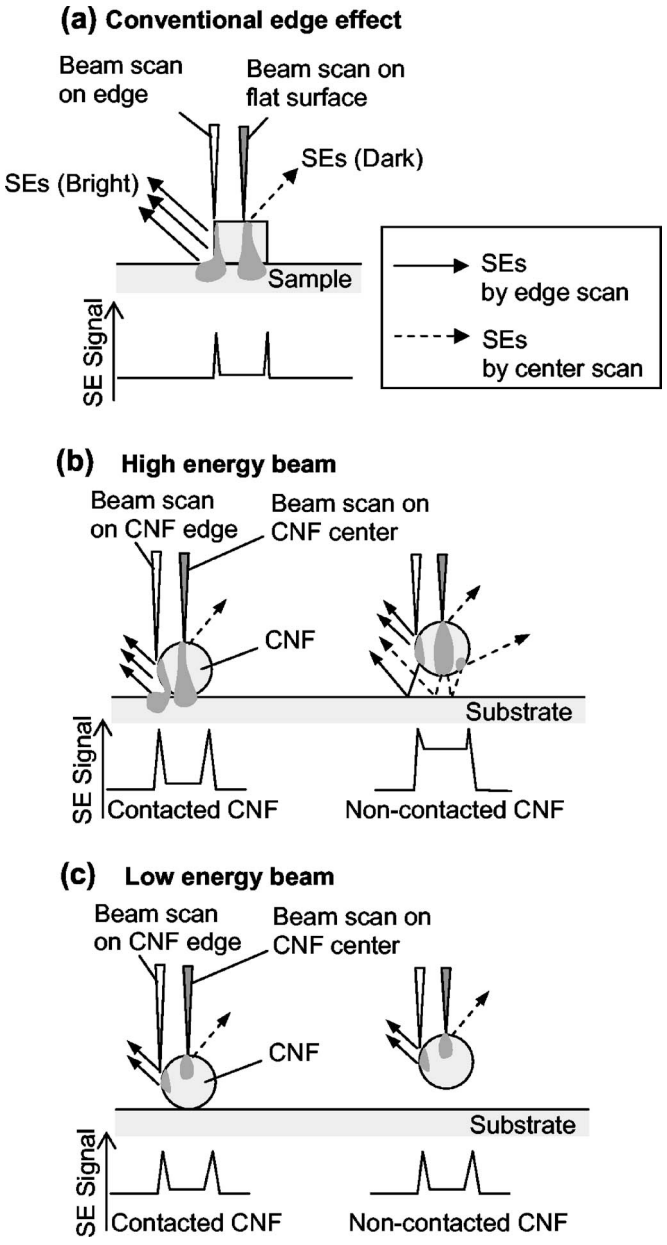

FIG. 4. Models of SE signal profiles. The solid arrows represent the secondary electrons (SEs) generated by beam scan on the edge, and broken arrows are SEs from the beam scan on the flat surface (a) or the center of CNFs [(b) and (c)]. (a) Conventional edge contrast mechanism. (b) Contrast mechanism for CNFs on a substrate, high energy case. (c) Contrast mechanism for CNFs on a substrate, low energy case.

To explain the image contrast observed above, we employ the SEM image formation mechanism of the edge of the sample.[16] In Fig. 4(a), a schematic of conventional edge contrast observed in SEM is shown. When the electron beam of a SEM is scanned over the sharp edge, more SEs are emitted (solid arrows) as compared to the flat surface (broken arrows). This is because only the SEs generated up to about 10 nm below the surface can be emanated from the sample, and when scanned over the edge, the incident beam travels a longer path near the surface area.[16] This mechanism leads to the sharp edge peaks in the SE signal, as shown in Fig. 4(a).

When applying this mechanism to CNFs on a substrate, similar image contrast is expected for the CNF contacted with the substrate [left panel of Fig. 4(b)]. On the other hand, in the case that the CNF has a slight gap between the substrate [right panel of Fig. 4(b)], even when the beam is scanned over the center of CNF, the electron beam penetrates the fiber and can produce more SEs from the bottom of the CNF and from the surface of the substrate below it. In addition, some of the backscattered or secondary electrons from the substrate can reflect back into the CNF and create tertiary electrons. All of these electrons contribute to restoring the SE signal when scanned over the center of the CNF (broken arrows) with the aid of efficient signal collection described above. Here we assume that the electron beam penetrates the CNF, corresponding to the case of a high energy beam. When the beam energy is lowered enough not to penetrate the CNF [Fig. 4(c)], however, the SE signal at the center of the CNF does not show the contrast change depending on whether or not the CNF is in contact with the substrate since the electron does not reach the substrate. For the low-energy case, the signal that provides bright contrast is dominated by SEs from the edges regardless of the CNF-substrate configuration, as shown in Fig. 4(c). This model explains well the SEM contrast observed in Figs. 1 and 2. In this model, the existence of the substrate below the CNF is essential, because the SE signal from the substrate and the tertiary electrons generated by the multiple scattering between CNF and the substrate account for the observed bright contrast. This can be understood by comparing the brightness of CNF edge of Fig. 1(b) with Fig. 1(d). A prominent edge peak observed in Fig. 1(b) disappears in Fig. 1(d) where the signal reflection from the substrate becomes weak.

To describe the diameter-beam energy correlation observed in Fig. 3, we define the threshold energy denoted as E_{th} for the observation of contrast change in the following way. Figure 5 shows the illustration of this procedure for the CNF of 250 nm diameter. First, the SE signal profiles corresponding to noncontacted area (denoted as A) and contacted area (B) are extracted from each image [Figs. 5(a) and 5(b)]. Then the normalized signal difference $(A-B)/(A+B)$ is calculated [Fig. 5(b)]. The value of $(A-B)/(A+B)$ is integrated with respect to the spatial position [horizontal axis in Fig. 5(b)]. The integrated value is plotted as a function of the beam energy [Fig. 5(c)]. Since the contrast becomes uniform at low beam energy, the signal difference is dropped at a certain range of energy, providing a reasonable estimate of threshold energy E_{th}. We define E_{th} as the midpoint between the onset and the end point of the drop, as shown in Fig. 5(c). We examined E_{th} for CNFs with various CNF diameters (d_{CNF}) ranging from 250 nm to the smallest 25 nm and with electron beam energy down to 100 eV. The relationship between the diameter d_{CNF} and the threshold energy E_{th} is plotted with filled circles in Fig. 6. Error bars correspond to the energy range between the onset and the end point of the signal difference drop shown in Fig. 5(c), reflecting the ambiguity of the definition of E_{th}. As expected, E_{th} increases monotonically with increasing diameter.

Threshold energy E_{th} can be correlated with the electron penetration depth derived from the electron penetration theory.[17] Electron beam penetration into the solid material is characterized by the successive elastic and inelastic scatter-

Downloaded 12 Feb 2008 to 129.210.95.1. Redistribution subject to AIP license or copyright; see http://jap.aip.org/jap/copyright.jsp

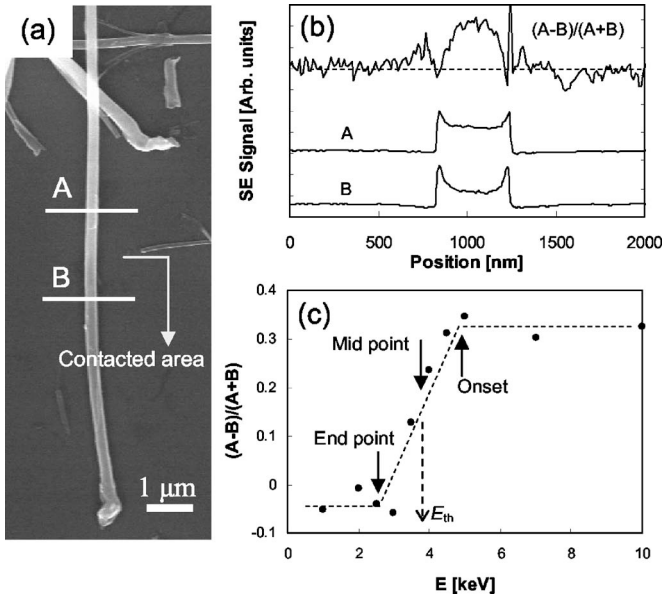

FIG. 5. Method for determination of threshold energy. (a) SEM image of the 250 nm diameter CNF captured by 10 keV beam energy. (b) SE signal profile along the lines *A* and *B* indicated in (a). $(A-B)/(A+B)$ shows normalized signal difference between *A* and *B*. The dotted line corresponds to zero for $(A-B)/(A+B)$. (c) Energy dependence of normalized signal difference for the 250 nm diameter CNF.

ings of electrons by the atoms, and the penetration depth of the electron beam is described by the universal formula of electron range,[17]

$$\rho R = aE^n, \tag{1}$$

where ρ is the mass density of material in units of $\mu g/cm^3$, R is the penetration depth (in units of cm) called the extrapolated electron range,[18] E is the energy of incident electron in units of keV, and a and n are dimensionless constants which are almost independent of the material used. Equation (1) shows that after experiencing multiple scatterings in the solid, the incident electrons travel close to the surface (the traveling distance corresponds to R) and emit SEs. The cross section for the SE emission is quite large, thus the bright contrast observed indicates that a large number of primary electrons with energy E have traveled a distance R and reached the surface area from which SEs generated can escape out of the sample. In other words, the SEM contrast has a very high correlation with the diffusion area of incident electrons.[16] As for the low-energy beam below 10 keV, $a=10.5$ and $n=1.38$ provide a good fit to the results for film penetration experiments in small atomic number materials.[19] By using these numbers and the density of graphite of $2.26\ g/cm^3$ for our CNF sample, we obtain the energy dependence of extrapolated electron range $R(E)$ as shown in Fig. 6. As can be seen, the experimental data fit well with the theory described by Eq. (1), confirming that electron penetration is the most relevant factor resulting in the observation of this unique SEM contrast. Although our analysis is based on the theory developed for bulk and foil samples,[17,19] and not necessarily for our quasi-one-dimensional nanofiber geometry, the use of Eq. (1) is justified because the geometry effect, if any, modifies the a and n values at most. More precise analysis of the electron scatterings and signal generation requires other approaches, including Monte Carlo technique,[20] where we can incorporate the realistic geometry of our nanofiber samples directly.

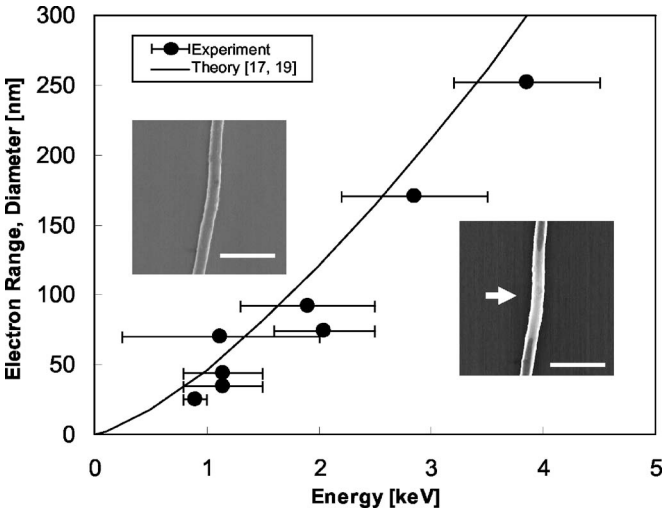

FIG. 6. Threshold energy dependence of CNF diameter (filled circles) and energy dependence of electron range (solid line). Error bars correspond to the energy width of the normalized contrast drop shown in Fig. 5(c). Insets: Typical contrast images in each graph region. Scale bar is 1 μm. The arrow in right inset indicates the position of bright contrast.

We also performed SEM imaging of CNFs on both metallic (Ni) and insulating (SiO_2 glass) substrates. The results are essentially the same as that performed on Si substrate, thus the mechanism is independent of the conductivity of the substrate used. This means that, in our experiment, neither the voltage contrast due to charging[12] nor EBIC effect[11] accounts for the SEM contrast observed here.

Finally, it should be noted that the present mechanism assumes that, when scanned over the center of the CNF, the electron diffusion area inside the CNF is elongated along the incident direction and the SE signal does not appear from the side of the CNF. Otherwise, the SE signal becomes less sensitive to the configuration of the bottom part of the CNF. This means that, for clear contrast observation, the lateral spread of electrons below the irradiated surface should be smaller than the penetration depth along the incident direction. This is the case for low atomic number materials such as carbon, where the large-angle elastic scattering cross section is small.[17] A similar study of SEM contrast for nanowires composed of heavier elements could further elucidate this mechanism.

IV. CONCLUSION

The contrast mechanisms of SEM imaging for analyzing the CNF-substrate interface have been presented. Bright contrast has been observed, reflecting the CNF's relative proximity to the substrate, when scanned with electron beam energy high enough to penetrate the CNFs. This behavior can be explained by the edge contrast of SEM image formation, and the threshold energy for contrast observation, as described by the theory of electron penetration in solids. This

Downloaded 12 Feb 2008 to 129.210.95.1. Redistribution subject to AIP license or copyright; see http://jap.aip.org/jap/copyright.jsp

knowledge can lead to the development of an efficient interface imaging method for all nanostructure devices, carried out without sample tilting.

ACKNOWLEDGMENTS

The authors are grateful to Takeshi Ogashiwa in Hitachi High-Technologies Corp., for invaluable discussion and Bill Roth in Hitachi High-Technologies America, Inc., for technical support.

[1]J. Kong, H. T. Soh, A. M. Cassell, C. F. Quate, and H. Dai, Nature (London) **395**, 878 (1998).
[2]B. A. Cruden, A. M. Cassell, Q. Ye, and M. Meyyappan, J. Appl. Phys. **94**, 4070 (2003).
[3]H. Cui, X. Yang, M. L. Simpson, D. H. Lowndes, and M. Varela, Appl. Phys. Lett. **84**, 4077 (2004).
[4]F. Kreupl, A. P. Graham, G. S. Duesberg, W. Steinhögl, M. Liebau, E. Unger, and W. Hönlein, Microelectron. Eng. **64**, 399 (2002).
[5]J. Li, Q. Ye, A. Cassell, H. T. Ng, R. Stevens, J. Han, and M. Meyyappan, Appl. Phys. Lett. **82**, 2491 (2003).
[6]A. Javey, J. Guo, M. Paulsson, Q. Wang, D. Mann, M. Lundstrom, and H. Dai, Phys. Rev. Lett. **92**, 106804 (2004).
[7]X. M. H. Huang, R. Caldwell, L. Huang, S. C. Jun, M. Huang, M. Y. Sfeir, S. P. O'Brien, and J. Hone, Nano Lett. **5**, 1515 (2005).
[8]E. Pop, D. Mann, J. Cao, Q. Wang, K. Goodson, and H. Dai, Phys. Rev. Lett. **95**, 155505 (2005).
[9]M. A. Kuroda, A. Cangellaris, and J. P. Leburton, Phys. Rev. Lett. **95**, 266803 (2005).
[10]M. Suzuki, Y. Ominami, Q. Ngo, K. Mcilwrath, K. Jarausch, A. M. Cassell, J. Li, and C. Y. Yang, Proceedings of 32th International Symposium for Testing and Failure Analysis, Texas, 12–16 November 2006 (unpublished).
[11]Y. Homma, S. Suzuki, Y. Kobayashi, M. Nagase, and D. Takagi, Appl. Phys. Lett. **84**, 1750 (2004).
[12]T. Brintlinger, Y. F. Chen, T. Dürkop, E. Cobas, M. S. Fuhrer, J. D. Barry, and J. Melngailis, Appl. Phys. Lett. **81**, 2454 (2002).
[13]M. D. Croitoru, G. Bertsche, D. P. Kern, C. Burkhardt, S. Bauerdick, S. Şahakalkan, and S. Roth, J. Vac. Sci. Technol. B **23**, 2789 (2005).
[14]Y. Ominami *et al.*, Appl. Phys. Lett. **87**, 233105 (2005).
[15]S. Takeuchi, A. Muto, M. Nakagawa, S. White, R. Tamochi, M. Sato, M. Yamada, and D. C. Joy, Microsc. Microanal. **10**, 950 (2004).
[16]H. Seiler, J. Appl. Phys. **54**, R1 (1983).
[17]K. Kanaya and S. Okayama, J. Phys. D **5**, 43 (1972).
[18]There are several definitions of the electron range. We employed the most studied one, extrapolated electron range, experimentally defined as the extrapolated onset of electron transmission through the thin film and theoretically defined as the maximum penetration depth.
[19]M. Kotera, K. Murata, and K. Nagami, J. Appl. Phys. **52**, 7403 (1981).
[20]M. Kotera, J. Appl. Phys. **65**, 3991 (1989).

Downloaded 12 Feb 2008 to 129.210.95.1. Redistribution subject to AIP license or copyright; see http://jap.aip.org/jap/copyright.jsp